Characterization of Airflow Distribution near Circuit Breaker Cu-Ag-Alloy Electrode Surface when It Breakdown

Jixing Sun *, Chenxi Shao , Kun Zhang , Jiyong Liu , Shengchun Yan , Liu Yang , Yan Zhang

Posted Date: 5 January 2024

doi: 10.20944/preprints202401.0505.v1

Keywords: Gas insulated schlieren method plasma contact structure breakdown airflow

Article

Characterization of Airflow Distribution near Circuit Breaker Cu-Ag-Alloy Electrode Surface when It Breakdown

Jixing Sun [1,*], Chenxi Shao [1], Kun Zhang [1], Jiyong Liu [1,2], Shengchun Yan [3], Liu Yang [2] and Yan Zhang [2]

[1] Beijing Jiaotong University, Haidian District, Beijing, 100044, China
[2] State Energy Group Shuohuang Railway Company, Suning 062350, China
[3] National Energy Group Shuohuang Railway Development Research Institute, Beijing 100080, China
* Correspondence: sanyou345@163.com; Tel.: +86-15801067328

Abstract: Circuit breakers are affected by multiple lightning strikes after the breaker has been tripped and can break down again, which will reduce the life of the circuit breaker and threaten the stable operation of the power system. Aiming at this problem, the paper obtained the temperature diffusion process of the inrush current process of circuit breaker opening and breaking through the schlieren technique, and combined with the existing image recognition technology to obtain the temperature characteristics of the airflow in the air gap of the contact, and the characteristics of the airflow flow. The results of the study show that the circuit breaker breakdown process generates a shock wave with a velocity approximately equal to the speed of sound under the same conditions. The maximum velocity of the airflow boundary diffusion is about 1/4 of the speed of sound under the same condition, and it decays very fast, reducing to the airflow drift velocity within 10ms after breakdown. The maximum temperature of the thermals is concentrated between 6000 and 8000 K and the temperature change is approximately inversely proportional to the square of time. The research provides the basis for the design of circuit breaker contact structure, opening speed optimization method, interrupter chamber and insulation design optimization.

Keywords: gas insulated; schlieren method; plasma contact structure breakdown airflow

1. Introduction

The circuit breaker will disconnect the contacts and remove the affected line when it senses overvoltage or high current during normal operation. According to the analysis report of circuit breaker breakdown accidents caused by lightning strikes in many places, after experiencing a lightning-induced trip, if the circuit breaker undergoes a lightning strike again during hot standby reclosure, a wave will undergo total reflection at the gap break of the dynamic and static contacts, generating a doubling of the lightning overvoltage and superimposing it on the industrial frequency power transmission voltage, causing the overall overvoltage level to exceed the insulation level of the circuit breaker's opening gap, resulting in breakdown of the circuit breaker's gap [1–5].

Regarding the arc models during the breakdown process of circuit breakers [2–7], different models have been proposed by Cassie A.M., Mayr O, L.S. Frost, and others. Cassie believes that the arc voltage remains approximately constant under high voltage conditions, and the arc energy is proportional to the rate of change of the arc cross-section. Mayr believes that under low current conditions, the arc is a cylinder with a constant diameter, and the dissipated power of the arc energy is approximately constant. L.S. Frost and others consider the arc to be equivalent to a plasma generator, explaining that the sudden drop in arc conductivity during current zero-crossing is caused by the thermal diffusion of the arc.

Regarding the gas jet process during the operation of circuit breakers, relevant research has been conducted by Lin Xin [7], Li Xinwen [8], and others. They found that intense turbulence is generated at the top of the electrodes during the arc burning process. Additionally, through simulation

Preprints (www.preprints.org) | NOT PEER-REVIEWED | Posted: 5 January 2024 doi:10.20944/preprints202401.0505.v1

experiments on the structural model of the arc extinguishing chamber, they obtained a series of data that are helpful for optimizing the design of circuit breaker arc extinguishing chambers [7–10].

Extensive research has been conducted by scientific research institutions such as the China Electric Power Research Institute, Beijing Jiaotong University, North China Electric Power University, and Shenyang University of Technology on the breakdown and recovery characteristics of insulation materials in circuit breakers [11–15]. The background of the research is the low current cutoff of capacitor bank switches, the expected breaking characteristics of 10kV rapid circuit breakers, and the pre-breakdown characteristics of 500kVGIS circuit breaker. There is currently no publicly available information or theoretical research on insulation breakdown and recovery processes between switch contacts under multiple lightning overvoltage conditions. Furthermore, there are no technical references or solutions available for related engineering issues, highlighting the urgent need for further research in this area [16,17].

Extensive research has been conducted on the recovery process of circuit breaker insulation under the influence of multiple lightning strikes. The paper utilized the schlieren method to capture the temperature diffusion process during the interruption of circuit breaker current. By combining existing image recognition technologies, the characteristic temperatures of the contact gap airflow and flow patterns were obtained. These findings provide a basis for the design of circuit breaker contact structures, optimization methods for interruption speed, as well as the optimization of arc extinguishing chambers and insulation design.

2. Thermal diffusion analysis of circuit breaker breakdown process

2.1. Electromagnetic thermal process model

Circuit breaker breakdown process is a multi-physical field coupling process, the circuit breaker breakdown process studied in this paper, the distribution of thermal airflow process selected electromagnetic-thermal, fluid heat transfer, fluid flow of these three physical fields for the model building and initial boundary conditions [17]. The first is the electromagnetic thermal process, where all domains of the model satisfy the current conservation equations.

$$\nabla \bullet J = Q_{J,V} \tag{1}$$

$$J = \sigma E + \frac{\partial D}{\partial t} + J_E \tag{2}$$

$$E = -\nabla V \tag{3}$$

where J is the current density, A/m^2, $Q_{J,V}$ is the charge density, C/m^3, E is the electric field strength, V/m, D is the potential shift, C/m^2, and V is the voltage, V.

The motion of the airflow field in the arc extinguishing chamber is more complex, and is described and constrained here by the N-S equation, which includes the equations of mass conservation, momentum conservation and energy conservation.

Mass conservation equation:

$$\frac{\partial \rho}{\partial t} + \frac{\partial \rho u}{\partial x} + \frac{\partial \rho v}{\partial y} + \frac{\rho v}{y} = 0 \tag{4}$$

Energy conservation equation:

$$\frac{\partial \rho e}{\partial t} + \frac{\partial \rho u(e + p/\rho)}{\partial x} + \frac{\partial \rho v(e + p/\rho)}{\partial y} + \frac{\rho v(e + p/\rho)}{y} = \frac{\partial (u\tau_{xx} + v\tau_{xy} + k\partial T/\partial x)}{\partial x} + \frac{\partial (u\tau_{xy} + v\tau_{yy} + k\partial T/\partial y)}{\partial y} + \frac{u\tau_{xy} + v\tau_{yy} + k\partial T/\partial y}{y} + Q \tag{5}$$

The parameters considered during the analysis include: ρ is the gas density, kg/m^3; p is the gas pressure, Pa; x is the axial displacement, m; y is the radial displacement, m; u is the axial velocity, m/s; v is the radial velocity, m/s; Q is the arc source term, J; e is the unit internal energy, J; τ is the viscous stress tensor; k is Boltzmann's constant, 1.38 × 10^{-23}J/K; and T is temperature, K. Considering

Preprints (www.preprints.org) | NOT PEER-REVIEWED | Posted: 5 January 2024 doi:10.20944/preprints202401.0505.v1

that the dynamic and static contacts are separated and the short electric arc between the contacts is a heat source, the non-isothermal flow equations corresponding to the fluid heat transfer module are set up here:

$$\rho C_p \frac{\partial T}{\partial t} + \rho C_p u \bullet \nabla T + \nabla \bullet q = Q + Q_p + Q_{vd} \tag{6}$$

$$q = -k\nabla T \tag{7}$$

$$\rho C_p \frac{\partial T}{\partial t} + \rho C_p u \bullet \nabla T + \nabla \bullet q = \nabla \bullet (k\nabla T) + \underset{\sim}{Q} \tag{8}$$

$$\underset{\sim}{Q} = \frac{\partial}{\partial T}(\frac{5k_B T}{2q})(\nabla T \bullet J) + E \bullet J + Q_{rad} \tag{9}$$

where C_P is the constant pressure heat capacity, J/(kg·K); Q_P is the heat source of warming, J; Q_{vd} is the heat source of loss, J; k_B is the solid thermal conductivity, W/(m·K); and Q_{rad} is the total volume radiation coefficient, W/m^3.

2.2. Analysis of the breakdown thermal diffusion process

Simulation experiments set the dynamic and static arc contact spacing is 14mm, SF6 gas pressure is 0.11MPa, refer to 1.1 modified control equations and boundary conditions, to obtain the temperature of the interrupter chamber at different moments, the temperature distribution cloud diagram shown in Figure 1a at 0.50119ms and in Figure 1b at 50.119s.

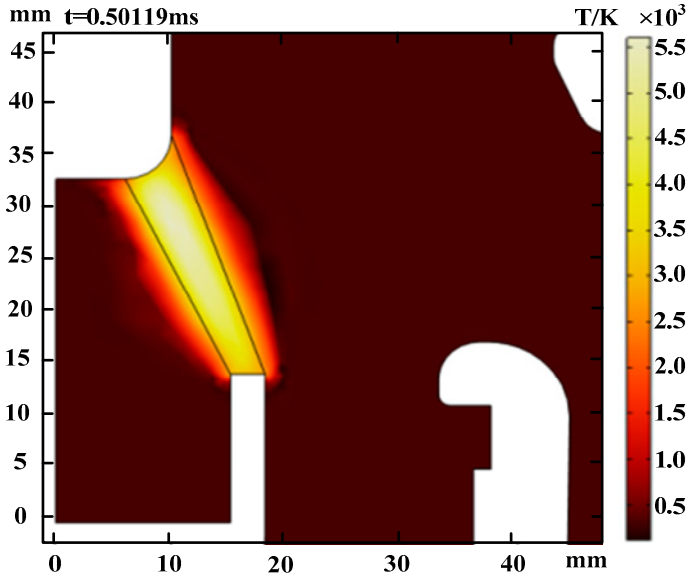

(**a**) Cloud view of the initial moment of ignition

Preprints (www.preprints.org) | NOT PEER-REVIEWED | Posted: 5 January 2024 doi:10.20944/preprints202401.0505.v1

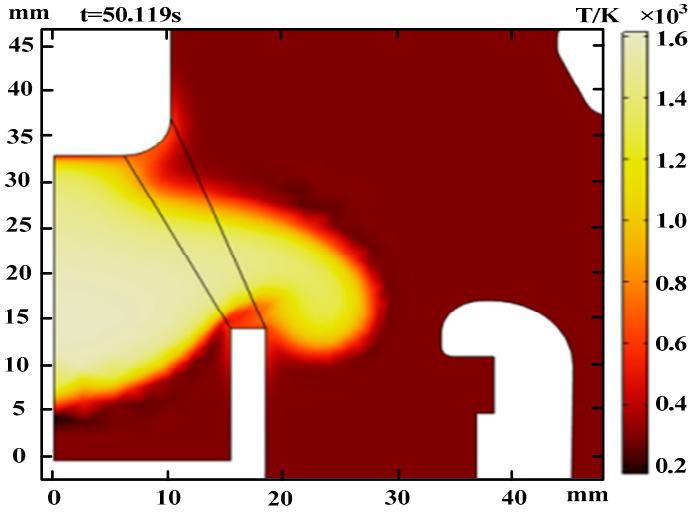

(**b**) Temperature distribution after 50ms

Figure 1. Airflow temperature distribution.

The velocity distribution cloud diagram were also gotten and shown in Figure 2(a) at 0.1 ms and in Figure 1(b) at150 ms.

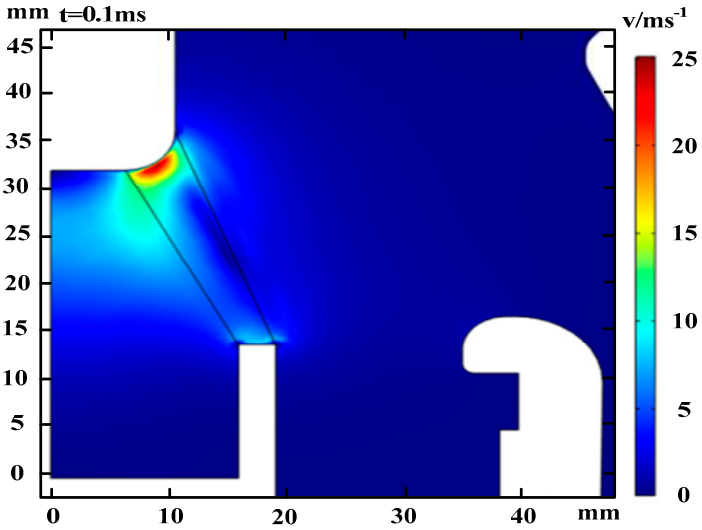

(**a**) Initial velocity of the plasma

Preprints (www.preprints.org) | NOT PEER-REVIEWED | Posted: 5 January 2024 doi:10.20944/preprints202401.0505.v1

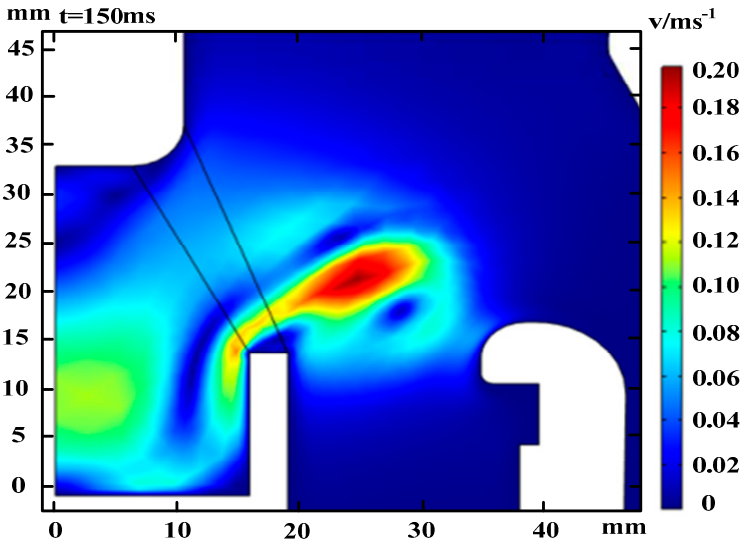

(**b**) Plasma velocity after 150ms

Figure 2. Airflow velocity distribution.

The temperature, motion speed and conductivity characteristics of the thermal airflow all reach the maximum value at the early moment after the discharge breakdown, and decrease sharply after the end of the discharge. The rate of change of the characteristic quantities is fastest at the early stage of the breakdown, and decreases gradually at the late stage of the breakdown. As shown in Figure 3, Figures 4 and 5.

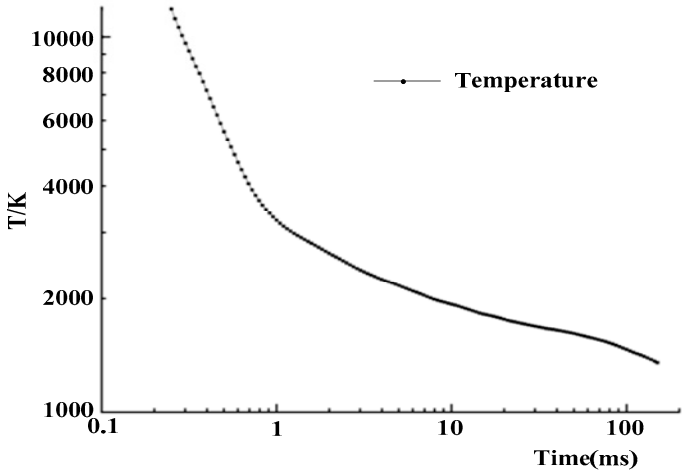

Figure 3. Temperature-time relationship.

Preprints (www.preprints.org) | NOT PEER-REVIEWED | Posted: 5 January 2024 doi:10.20944/preprints202401.0505.v1

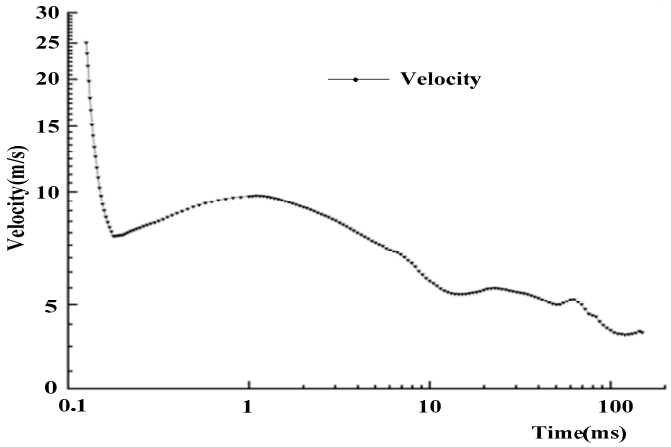

Figure 4. Velocity-time graph of the thermal airflow.

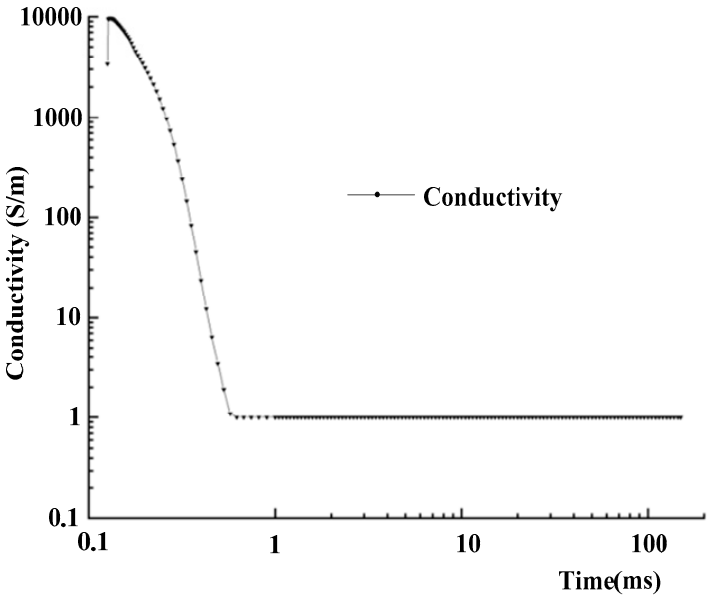

Figure 5. Conductivity-time relationship.

3. Breakdown process and thermal process test research

3.1. Experimental procedure

The gas-insulated circuit breaker breakdown experimental platform is mainly composed of three parts: adjustable gap circuit breaker experimental device (shown in Figure 6), lightning overvoltage generator, and ripple image acquisition device (schematic diagram shown in Figure 7).

Preprints (www.preprints.org) | NOT PEER-REVIEWED | Posted: 5 January 2024 doi:10.20944/preprints202401.0505.v1

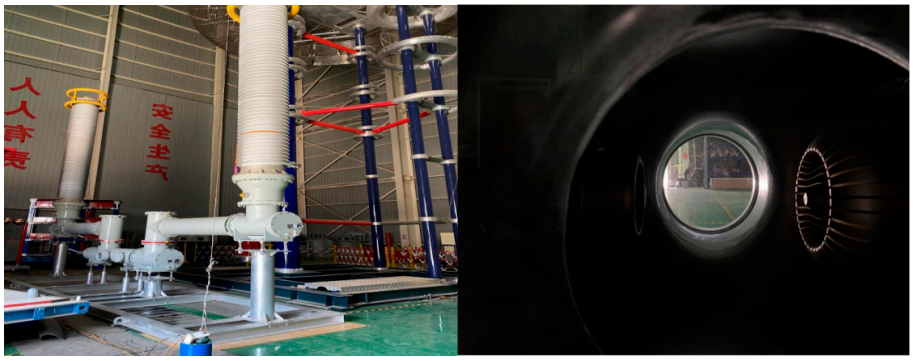

Figure 6. The test sample and the Gap.

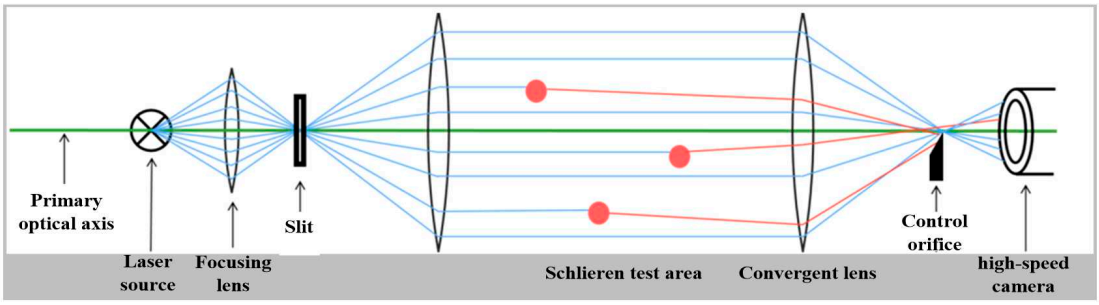

Figure 7. Working principle of schlieren device.

Firstly, according to table 1, adjust the contact spacing and then the output current of the impact current generator is continuously adjusted to finally obtain the circuit breaker breakdown current under different air pressure conditions.

Table 1. Test results of impulse withstand voltage.

Arc contact spacing/cm	Breakdown current/kA
0.6	10.357
0.8	12.092
0.9	13.857
1.0	13.861
1.2	15.452
1.4	16.632

3.2. Study on the development speed of thermal air flow

Analyzing the ripple images of the same air pressure with different electrode spacing, the approximate rectangular image in the center of each image is the ripple outline of the moving contact, the trapezoidal bulge in the center of the right side of the moving contact is the ripple outline of the moving arc contact, and the space between the moving contact and the arc-shaped observation window on the right side of the image is the air gap for discharging, and the moments of shooting in the demonstration pattern from left to right and from top to bottom were approximated to be in the exponential increment.

The pixel length occupied by the diameter of the moving arc contact in the grain image is about 679 pixels long, and the conversion ratio is 0.1296mm for 1 pixel point to the actual length.

$$d_0 = \frac{d_h}{N_0 \times N_h} = \frac{88}{1 \times 679} = 0.1296 \tag{10}$$

Preprints (www.preprints.org) | NOT PEER-REVIEWED | Posted: 5 January 2024 doi:10.20944/preprints202401.0505.v1

In the equation, d_0 is the actual length represented by the unit pixel, mm; dh is the actual length of the moving arc contact design, mm; N0 is the number of unit pixels, and N_h is the average pixel percentage of the moving arc contact.

The breakdown process and schlieren image data is shown in figure 8, It is calculated that the speed of sound in SF6 gas is 135.38m/s under the temperature of 300K and the pressure of SF6 gas is 0.11MPa, and the propagation speed of the excitation wave within 1ms after the discharge is measured at the above sampling point is up to 141.35m/s, which is about the same as the speed of sound in SF6 under the condition.

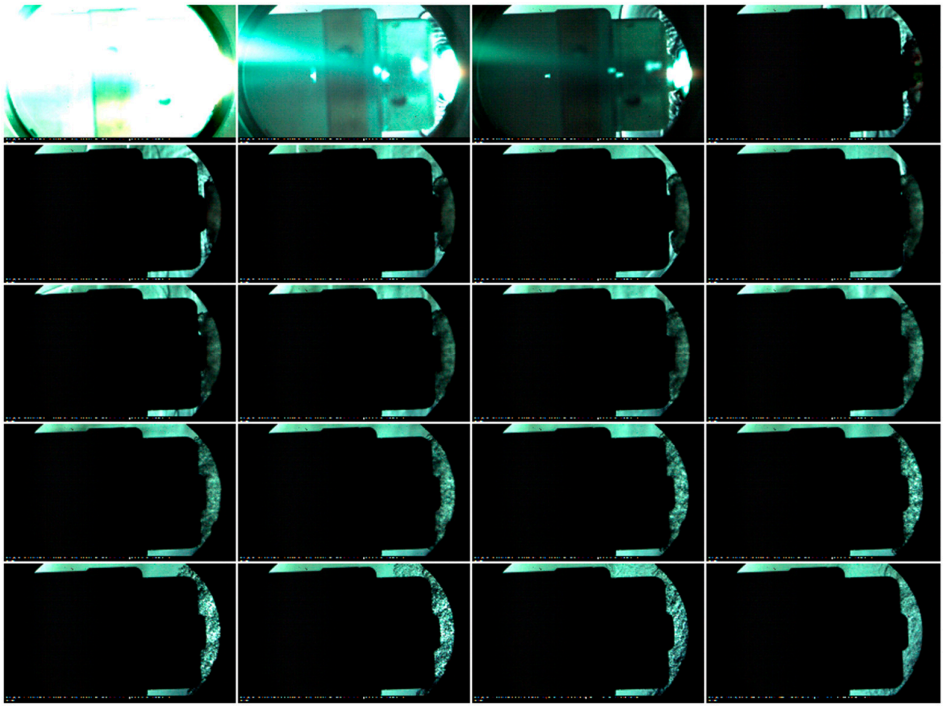

Figure 8. Sequential display of schlieren image data.

3.3. Calculation of the boundary temperature of the thermal air flow

Extraction of thermal airflow motion characteristics is mainly aimed at thermal airflow in different frame rates under the characteristics of airflow boundary diffusion, locating different boundaries of the arc segment diffusion sampling analysis, shown in Figure 9.

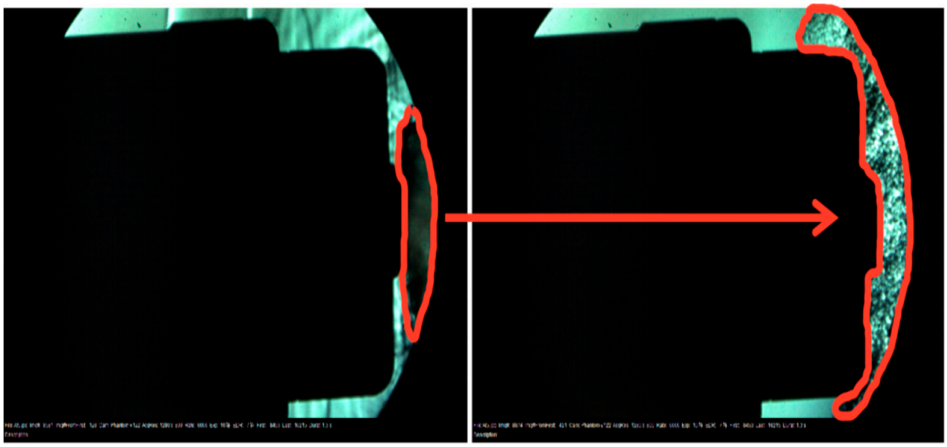

Figure 9. Thermal flow boundary diffusion.

Preprints (www.preprints.org) | NOT PEER-REVIEWED | Posted: 5 January 2024 doi:10.20944/preprints202401.0505.v1

MATLAB was first used to convert the image data into gray scale matrix data as shown in Figure 10, and the airflow motion boundaries were calibrated using the gray scale values corresponding to the unbroken image and standard temperature values.

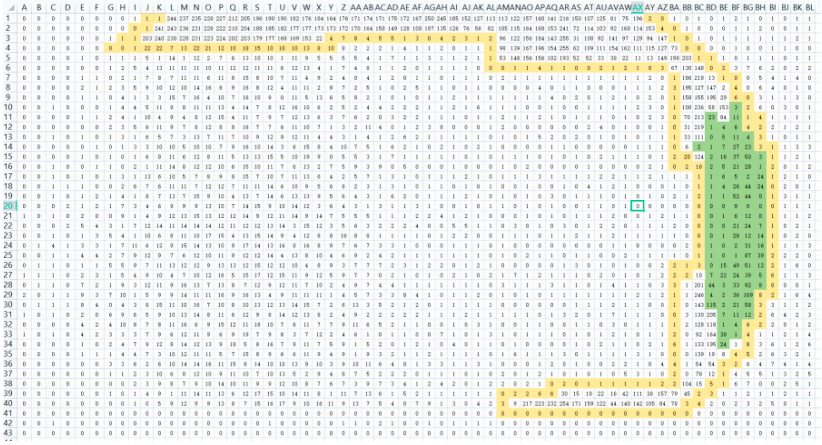

Figure 10. Getting grayscale matrix.

Based on this method, the hot gas stream boundary temperature development characteristics are obtained, the hot gas stream temperature reaches the level of 5000K at the end of the discharge about 1ms, and basically maintains below 1000K and decreases at a relatively slow rate after 10ms at the end of the discharge, shown in figure 11 and at the same time, it presents similar oscillatory tendency with the movement of the hot gas stream on the logarithmic scale, and the oscillatory period of the gas stream temperature is similar to that of the gas stream velocity on the logarithmic scale, but the amplitude of the data oscillations is much smaller, it is due to the fact that, compared to the mass inertia of gas, the thermal inertia of the gas is much larger than that of it, and the damping of the temperature system is much larger than that of the motion system, therefore, the amplitude of the temperature characteristics of the oscillations is much lower.

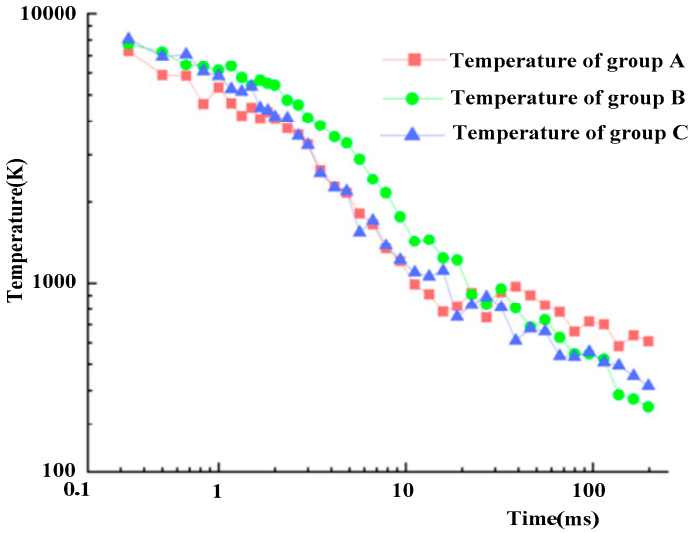

Figure 11. Temperature of groups A, B and C.

Through the corresponding conversion of the thermal plasma conductivity versus time curves, the conductivity characteristics of the air-gap thermal gas flow at different moments can be obtained. The thermal conductivity of the gas flow reaches the maximum value at the initial moment after the breakdown of the discharge and decreases rapidly after the end of the discharge, and the rate of change of the characteristic quantity is the fastest at the initial stage of the breakdown, and gradually

Preprints (www.preprints.org) | NOT PEER-REVIEWED | Posted: 5 January 2024 doi:10.20944/preprints202401.0505.v1

decreases at the later stage of the breakdown, shown in figure 12. The analysis results are consistent with the theoretical analysis.

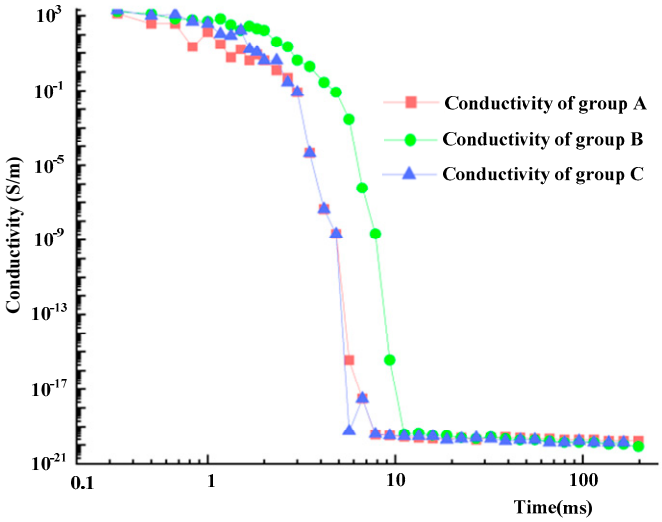

Figure 12. Conductance feature of the airflow.

4. Conclusions

The paper aims at the problem of electrothermal re-breakdown during the opening process of circuit breaker, studies the temperature diffusion process during the inrush current process of circuit breaker opening and breaking based on the schlieren method, and combines the existing image recognition technology to obtain the temperature characteristics of the airflow in the air gap of the contacts, the characteristics of the airflow flow. Specific conclusions were obtained as follows:

(1) At the early stage of circuit breaker breakdown and discharge, the surge wave speed is approximately maintained at the speed of sound in the ambient condition, and the movement speed of the hot airflow shows the decay characteristic which is inversely proportional to the square of the time, and the speed of the airflow at the observable initial moment is 34.33m/s at the maximum, and the maximum airflow diffusion speed is 22.79m/s at the electrode spacing of 1.0cm.

(2) The temperature of the hot gas stream is 8051K at the end of the discharge process, and the maximum value of the gas stream diffusion velocity is 8051K when the electrode spacing is 1.0cm under SF6 gas pressure of 0.11MPa. Meanwhile, under the exponentially decreasing temperature change with time.

(3) The hot gas conductivity is affected by the plasmonization of the gas, and the insulating property of the gas has been fully recovered when the temperature is lower than 3500K, i.e., the electrical insulation strength of SF6 has basically been recovered about 10ms after the end of the discharge, and the trend of recovery of the insulation strength of different groups tends to be the same.

Acknowledgments: The authors would like to thank reviewers for their pertinent comments that help to improve the quality of this paper. This work was supported by the National Natural Science Foundation of China 52377131), Science and Technology Project of National Energy Group (SHTL-21-08, SHSN-22-05, SHTL-2022-9, SNFZ23086).

References

1. Xiangzheng Xu,Wenguang Hu. Modeling and simulation of arc grounding fault of middle and low voltage distribution network based on ATP-EMTP, Journal of Computational Methods in Sciences and Engineering,2020,20(4).
2. B.R. Brown and S.M. Mahajan,"Circuit-Based Mathematical Model of an Arc Heater for Control System Development"in IEEE Access, vol.9, pp.143085-143092,2021, doi: 10.1109 / ACCESS . 2021 . 3121189.
3. L. S. Frost,A Lee. Interruption Capability of Gases and Gas Mixtures in a Puffer-Type Interrupter, IEEE Transactions on Plasma Science,1980,8(4).

4. Robin-Jouan P, Yousfi M. New Breakdown Electric Field Calculation for SF6 High Voltage Circuit Breaker Applications, Plasma science & technology, 2007,9: 690.
5. X. J, X. L, H. Z, et al. Analysis of the Dielectric Breakdown Characteristics for a 252-kV Gas Circuit Breaker [J]. IEEE Transactions on Power Delivery, 2013,28(3): 1592-1599.
6. A. L, C. D, F. F, et al. Three-Dimensional Unsteady MHD Modeling of a Low-Current High-Voltage Nontransferred DC Plasma Torch Operating With Air [J]. IEEE Transactions on Plasma Science, 2011,39(9): 1889-1899.
7. Song Yu, Lin Xin, Zhou Tao, Wang Feng, Simulation of Airflow Field and Breaking Capacity of 550 kV Fast Circuit Breaker, High Voltage Engineering, 2023,49(6): 2432-2441.
8. Zhang Yu, Lü Qishen, Xiang Zhen, Guo Ze, Li Xingwen, Influence of Frequency on Arcing Characteristics of High-voltage Puffer SF6 Circuit Breaker, High Voltage Engineering, 2023,44(12): 3987-3994.
9. Jixing Sun, Kun Zhang, Kaixuan Hu, Jiyong Liu,, Yu Tian,, Xin Wang, and Shengchun Yan, Evolution of Elements on Electrode Surfaces in Gas-Insulated Systems under Electrical Heating, Coatings, 2023, 13, 33.
10. R. C, K. F, H. L. On the Partial Difference Equations of Mathematical Physics [J]. IBM Journal of Research and Development, 1967,11(2): 215-234.
11. Jixing Sun, Yongzhi Fan, Kun Zhang, Jiyong Liu, Xin Wang and Shengchun Yan, The Leakage Current Characteristics of High-Gradient MOA Plate and Its Heating Analysis with Coatings under High-Frequency Overvoltage, Coatings, 2023, 13, 497.
12. H. Y, M. L. Multiple-parameter quantum estimation and measurement of nonselfadjoint observables [J]. IEEE Transactions on Information Theory, 1973,19(6): 740-750.
13. X. J, X. L, H. Z, et al. Analysis of the Dielectric Breakdown Characteristics for a 252-kV Gas Circuit Breaker [J]. IEEE Transactions on Power Delivery, 2013,28(3): 1592-1599.
14. S. A R, R. K, M. M R. Estimation of Gas Discharge Rates in EHV Gas Circuit Breakers: 2019 International Conference on High Voltage Engineering and Technology (ICHVET) [C], 2019.
15. H. U, M. K, Y. O, et al. Measurement of hot gas exhaust characteristics in SF6 circuit breaker with small model interrupter: 2013 2nd International Conference on Electric Power Equipment - Switching Technology (ICEPE-ST) [C], 2013.
16. M. T, H. U, Y. Y. Method of Evaluating Exhaust Characteristics of High-Voltage Circuit Breaker [J]. IEEE Transactions on Power Delivery, 2020,35(2): 707-714.
17. V. V, Z. V, J. S. Analysis of breaking capability within asymmetrical short circuits: 2015 16th International Scientific Conference on Electric Power Engineering (EPE) [C], 2015.
18. Sun Jixing, Song Sibo, Li Xiyu, Lv Yunlong, Ren Jiayi, Ding Fan, Guo Changwang, Restraining Surface Charge Accumulation and Enhancing Surface Flashover Voltage through Dielectric Coating [J], Coatings, 2021, 11(7): 11070750.